



## Article

# PS-InSAR Based Monitoring of Land Subsidence by Groundwater Extraction for Lahore Metropolitan City, Pakistan

Muhammad Afaq Hussain <sup>1,\*</sup>, Zhanlong Chen <sup>1,\*</sup>, Ying Zheng <sup>1</sup>, Muhammad Shoaib <sup>2</sup>, Junwei Ma <sup>3</sup>, Ijaz Ahmad <sup>4</sup>, Aamir Asghar <sup>5</sup> and Junaid Khan <sup>6</sup>

<sup>1</sup> School of Geography and Information Engineering, China University of Geosciences, Wuhan 430074, China

<sup>2</sup> State Key Laboratory of Hydraulic Engineering, Simulation and Safety, School of Civil Engineering, Tianjin University, Tianjin 300072, China

<sup>3</sup> Badong National Observation and Research Station of Geohazards, China University of Geosciences, Wuhan 430074, China

<sup>4</sup> Pakistan Atomic Energy Commission, Islamabad 44000, Pakistan

<sup>5</sup> Institute of Mountain Hazards and Environment, CAS, Chengdu 610041, China

<sup>6</sup> Faculty of Engineering, China University of Geosciences, Wuhan 430074, China

\* Correspondence: chenlz@cug.edu.cn

**Abstract:** Groundwater dynamics caused by extraction and recharge are one of the primary causes of subsidence in the urban environment. Lahore is the second largest metropolitan city in Pakistan. The rapid expansion of this urban area due to high population density has increased the demand for groundwater to meet commercial and household needs. Land subsidence due to inadequate groundwater extraction has long been a concern in Lahore. This paper aims to present the persistent scatterer interferometry synthetic aperture radar (PS-InSAR) technique for monitoring the recent land subsidence in Lahore, based on the Sentinel-1 data obtained from January 2020 to December 2021. PS-InSAR techniques are very efficient and cost-effective, determining land subsidence and providing useful results. Areas of high groundwater discharge are prone to high subsidence of  $-110$  mm, while the surroundings show an uplifting of  $+21$  mm during the study period. The PS-InSAR study exposes the subsidence area in detail, particularly when the subsoil is characterized by alluvial and clay deposits and large building structures. This type of observation is quite satisfactory and similar to ground-based surface deformation pertinent to a high subsidence rate. Results will enable more effective urban planning, land infrastructure building, and risk assessment related to subsidence.

**Keywords:** Lahore; PS-InSAR; Sentinel-1; SAR images; land subsidence



**Citation:** Hussain, M.A.; Chen, Z.; Zheng, Y.; Shoaib, M.; Ma, J.; Ahmad, I.; Asghar, A.; Khan, J. PS-InSAR Based Monitoring of Land Subsidence by Groundwater Extraction for Lahore Metropolitan City, Pakistan. *Remote Sens.* **2022**, *14*, 3950. <https://doi.org/10.3390/rs14163950>

Academic Editor: Christian Bignami

Received: 29 July 2022

Accepted: 12 August 2022

Published: 14 August 2022

**Publisher's Note:** MDPI stays neutral with regard to jurisdictional claims in published maps and institutional affiliations.



**Copyright:** © 2022 by the authors. Licensee MDPI, Basel, Switzerland. This article is an open access article distributed under the terms and conditions of the Creative Commons Attribution (CC BY) license (<https://creativecommons.org/licenses/by/4.0/>).

## 1. Introduction

Land subsidence (LS) is a geological disaster caused by human and natural processes such as compaction of unconsolidated layers, loose sediment settlement, and overutilization of subsurface resources [1]. It is generally a slower process that is difficult to detect in its early stages. If the subsidence occurs, it might result in a gradual decline in land surface level, causing major economic disruption [2,3]. LS happens in over 150 nations worldwide, notably in heavily populated urban regions such as major cities in China [4–11], India [12,13], Turkey [14,15], Iran [16–18], Italy [19–22], Japan [23,24], Mexico [25,26], Indonesia [27,28], and Pakistan [29–32], with severe consequences and triggered effects. There is growing concern about environmental hazards created by uncontrolled urbanization as cities develop and grow rapidly. Environmental pollution, water, air, soil quality, and waste management have been significant study fields. However, subsurface environmental risks are becoming a substantial issue in Asian cities. The surface environmental status of the region is closely related to urban development and building activity [33–35].

LS is one of the most severe underground environmental hazards, posing a higher risk for human and economic losses [36]. Monitoring long-term land subsidence spatial and

temporal evolution is crucial for executing remedial measures and disaster alerts for such essential engineering structures to reduce possible destruction [37,38]. LS can be caused by chemical changes and natural processes under the earth's surface, although these processes are incredibly gradual. Subsidence caused by human activity forces, on the other hand, such as construction activities, mining, and groundwater extraction, are occurring at a higher pace and have a more significant impact on LS. Land subsidence is not a recent concept, but its effects have been more severe due to centralized urbanization, which has confined development. Thus, a disaster in these areas can result in significant losses. LS is a worldwide dispersed occurrence, and its causes and origin were comprehensively and exclusively defined in the literature [39]. Land subsidence risk is best measured over intensive land displacement checks, incorporating uplift and subsidence. Several investigations have revealed that both of these procedures occur together [20]. Earlier, expensive and prolonged methods such as Global Positioning System (GPS) and leveling techniques were employed [40]. However, Synthetic Aperture Radar (SAR) techniques have proven to be an adequate substitute for studying land subsidence [41]. InSAR techniques have been utilized efficiently in LS research. The InSAR technique employs repeat pass radar imagery from airborne or space detectors [42].

InSAR has been an efficient geodetic surveying methodology over the last few years compared to traditional ground-based sparse point analytical techniques. It can identify a planar measurement to a vast extent with cheap cost and high accuracy [43,44]. However, the typical InSAR approach is severely constrained by spatial and temporal deconvolution and atmospheric delay induced by varied satellite orientations, atmospheric variations, and long acquisition intervals [45]. As a result, PS-InSAR [46] was designed to overcome the incoherence restriction of the standard InSAR approach across long time intervals and vast regions. The PS-InSAR can improve and modify the assessment of subsidence, decreasing it from 10 to 20 mm to 2–3 mm [47]. Advanced methodology belongs to a subclass of multi-temporal InSAR methods that enable us to recover the proceeds of ground displacement at millimeter precision. Because artificial amenities and buildings give higher density PS locations and considerably increase the interferograms' signal-to-noise ratio, the PS-InSAR approach benefits urban land subsidence detection [48]. PS-InSAR is extensively used in Beijing [49–51], Algeria [52], London [53,54], Mashhad (Middle East) [55], Los Angeles [56], Spain [57], coastal areas of Africa [58], and Poland [59] to detect LS using Sentinel-1 data in metropolitan regions.

This study was conducted to record ground subsidence in Lahore, Pakistan, from 10 January 2020 to 30 December 2021 and 2 January 2020 to 22 December 2021, using descending and ascending tracks. The satellite can see the same target region from different sites, with incidence angles that range from horizontal ( $\sim 45^\circ$ ) to vertical ( $\sim 23^\circ$ ) [60] in the E–W direction. Ascending and descending path images enhance the understanding of displacement and visualization from different sites [61]. Furthermore, our work evaluates the PS-InSAR technique's capability for LS studies in metropolitan areas [62,63]. In this study, we: (1) employed both descending and ascending tracks using Sarproz software, (2) used Sentinel-1 SAR data to estimate line of sight (LOS) and vertical deformation in the present research compared to previous studies on Lahore city, and (3) calculated the rate of subsidence in recent years (2020–2021). The findings will enable more effective planning, surface infrastructure building, and risk management related to subsidence in the research area.

## 2. Materials and Methods

### 2.1. Study Area

Figure 1 depicts the study area, which includes the city of Lahore and its surroundings. Lahore, Pakistan's second-biggest city in Punjab, surrounded by India on the east and the Kasur district on the south, is located near the Ravi River. Lahore is the world's 34th largest city, with a population of 13.5 million people. It is located at an elevation of 682 to 698 m above mean sea level. It covers an area of 1014 km<sup>2</sup> (Figures 1 and 2).

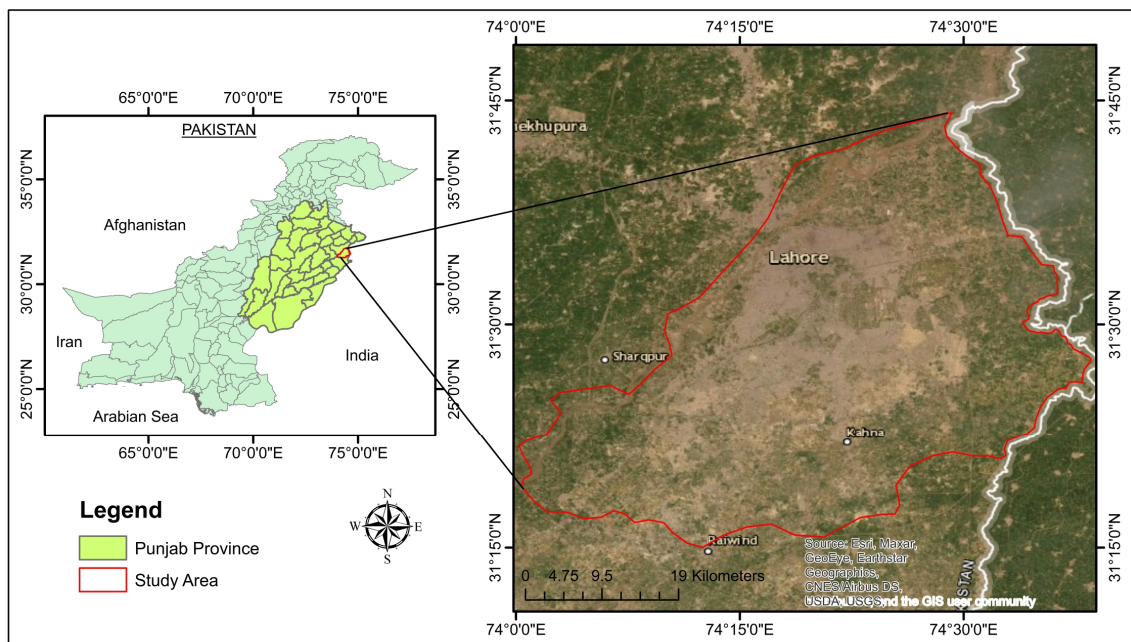


Figure 1. The location of the research area.

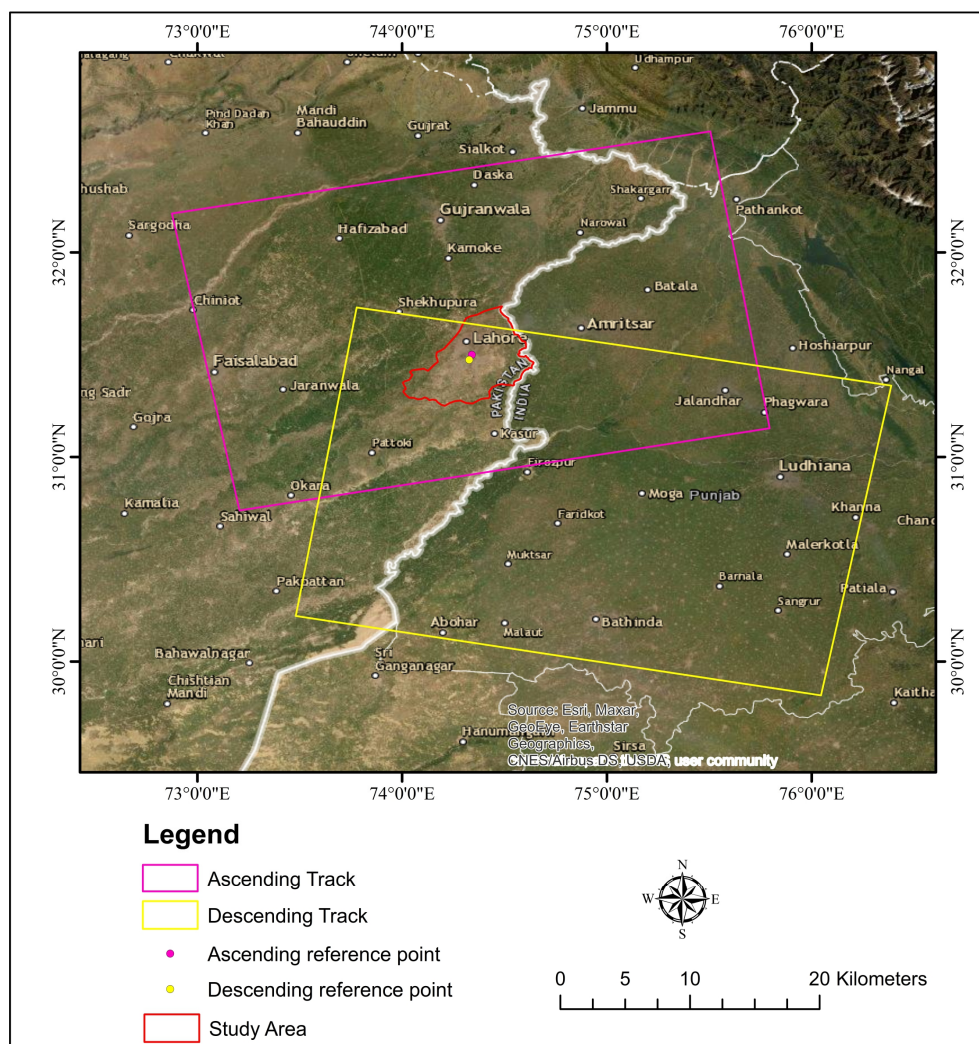
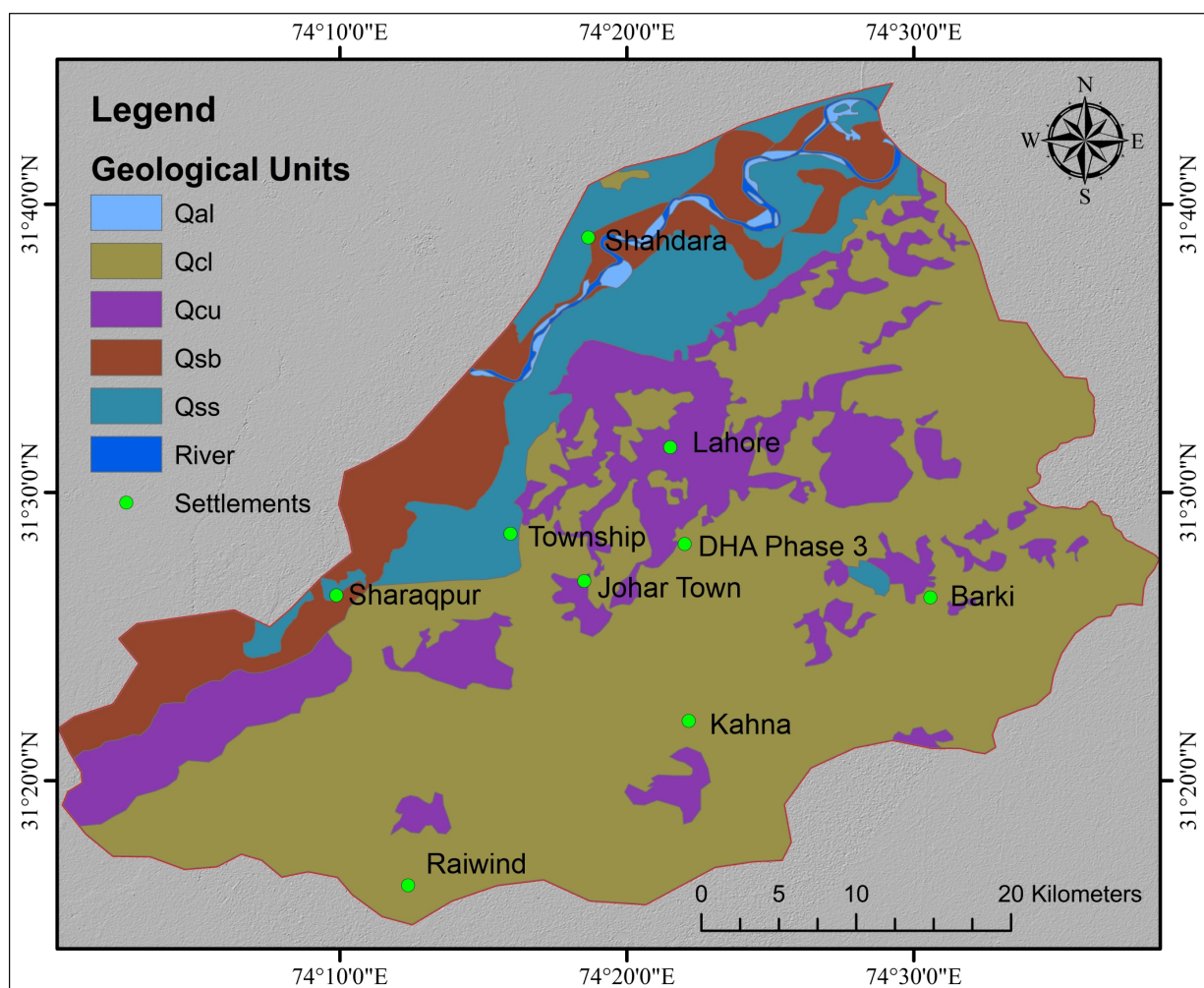


Figure 2. The study area (red color) with the reference points and footprint of the master region.

Lahore is relatively flat, with a 1:3000 average gradient sloping south and southwest. It is separated into two sections: the low-lying territory along the Ravi River and the comparably highland area in the east away from the Ravi [64]. During monsoon floods, the lowlands are typically swamped by river water. The Ravi River runs west of Lahore District, establishing a border with Sheikhpura District [64]. Lahore has a hot semi-arid steppe climate with significant seasonal changes in temperature and rainfall (Pakistan Meteorological Department). The average yearly temperature is around 24 °C, fluctuating from 36 °C in summer to 12 °C in winter. The highest temperature measured in Lahore was 48 °C (118 °F) on 9 June 2007, while the lowest was −1 °C in January 1968. The mean yearly rainfall is 675 mm, with variations ranging from 300 to 1200 mm. The most precipitation (221 mm) was reported on 13 August 2008.

## 2.2. Geology of the Area

Lahore is situated in the Indus Basin's alluvial plain, on the left bank of the Ravi River. According to research conducted in 1961–1962, the Lahore region is overlaid by a substantial width of alluvial sediments, reaching up to 300 m in depth. The sediments have a thickness larger than 300 m and are made of unconsolidated alluvial deposits in various quantities of sand, silt, and clay (Figure 3). The primary soil type in this region is alluvial; even though it is a type of soft soil, the region is prone to geohazards [65].



**Figure 3.** Geological map of study area overlying on hillshade map: Qal: recent deposits of Ravi River; Qcl: brown silt, clay, and sand; Qcu: meander-belt deposit; Qsb: meander-belt of deposit of Ravi River, Qss: younger flood plain deposit; river.

### 2.3. Dataset

This study used Sentinel-1 (C-band) SAR images captured along descending and ascending orbits (Alaska Satellite Facility: <https://asf.alaska.edu/about-asf/> (accessed on 20 January 2022)). Sentinel-1 data was chosen because this mission offers long-term, timely data with adequate resolution at no cost. These data provide a valid source for studying deformation and its progression through time, which may be utilized to forecast future situations. The PSI usually requires 20 SAR images [66] to analyze C-band data. The PSI measures surface displacement over a year, considering atmospheric, signal noise and topographic influences [67]. This sensor has a ground resolution of nearly 5 m in the range and 20 m in azimuth [68]. This sensor has numerous acquisition modes, comprising strip map (SM) and interferometric wide (IW). When the IW mode was compared to other acquisition techniques, it was observed that the IW mode required additional data manipulation for image co-registration with high accuracy of up to 0.001 pixels [52]. This research obtained 41 images from the ascending path number 100 (2 January 2020–22 December 2021) and 38 from the descending path number 34 (10 January 2020–30 December 2021). The properties of Sentinel-1 datasets and the parameters used in this research are detailed in Table 1.

**Table 1.** Properties of Sentinel-1 datasets and their parameters.

Data Information	Ascending	Descending
Product type	Sentinel 1 IW SLC	
Polarization	VV + VH	
No. of images	41	38
Time period	2 January 2020–22 December 2021	10 January 2020–30 December 2021
Track	100	34
Frame	99	487
Coverage (km <sup>2</sup> )	250	
Incident angle	horizontal (~45°) to vertical (~23°)	
Range (m)	5	
Azimuth resolution (m)	20	

This study used Sarproz (<https://www.sarproz.com/sarproz-faq> (accessed on 15 April 2022)) software, which is commercial and extremely useful for SAR data analyses software [52]. Zhu et al. found land subsidence in Beijing induced by groundwater extraction using Persistent Scatterer Interferometry (PSI) with SAR Dataset [69]. The PS-InSAR technique concepts are described in [70].

### 2.4. Data Processing

Data preparation, analysis of data, atmospheric phase screen APS calculation, and multi-image analysis were all part of the PS-InSAR process. The data analysis in the study is shown in Figure 4.

The PS-InSAR method examines time series SAR data. The approach focuses on speckle-free, steady, point-like scatterers that produce a definite result. These are persistent scatterers (PS), which provide a consistent phase history across the acquisition time span. The PS phases are stable over time and do not exhibit temporal decorrelation, allowing for long-term observation and monitoring of displacement. The interferometric phase  $\varphi_{Int}$  of SAR signal of wavelength ( $\lambda$ ) between two distinct images is represented as:

$$\varphi_{Int} = \varphi_{topography} + \varphi_{movement} + \varphi_{orbit} + \varphi_{atmosphere} + \varphi_{noise} \quad (1)$$

where  $\varphi_{topography}$  is the variation in phase caused by height errors,  $\varphi_{orbit}$  is the error produced due to phase triggered by errors due to orbit estimation,  $\varphi_{movement}$  is the component generated by terrain displacement in the LOS path between two SAR acquisitions, and  $\varphi_{atmosphere}$  is the phase component as a result of variations in atmospheric phase delay. Finally,  $\varphi_{noise}$  refers to phase noise, including thermal noise and other error components.

Importing single look complex data with precise tracks is one of the data preparation analysis steps. For this investigation, ascending imagery with the same rotations was used. Images were polarized depending on path information, and slave and master images were selected. The study region's master images were obtained first, accompanied by slave images overlaying the same entire region as the master image. This scenario created a star graph between the master and slave images (Figure 5). A specific area was co-registered and examined.

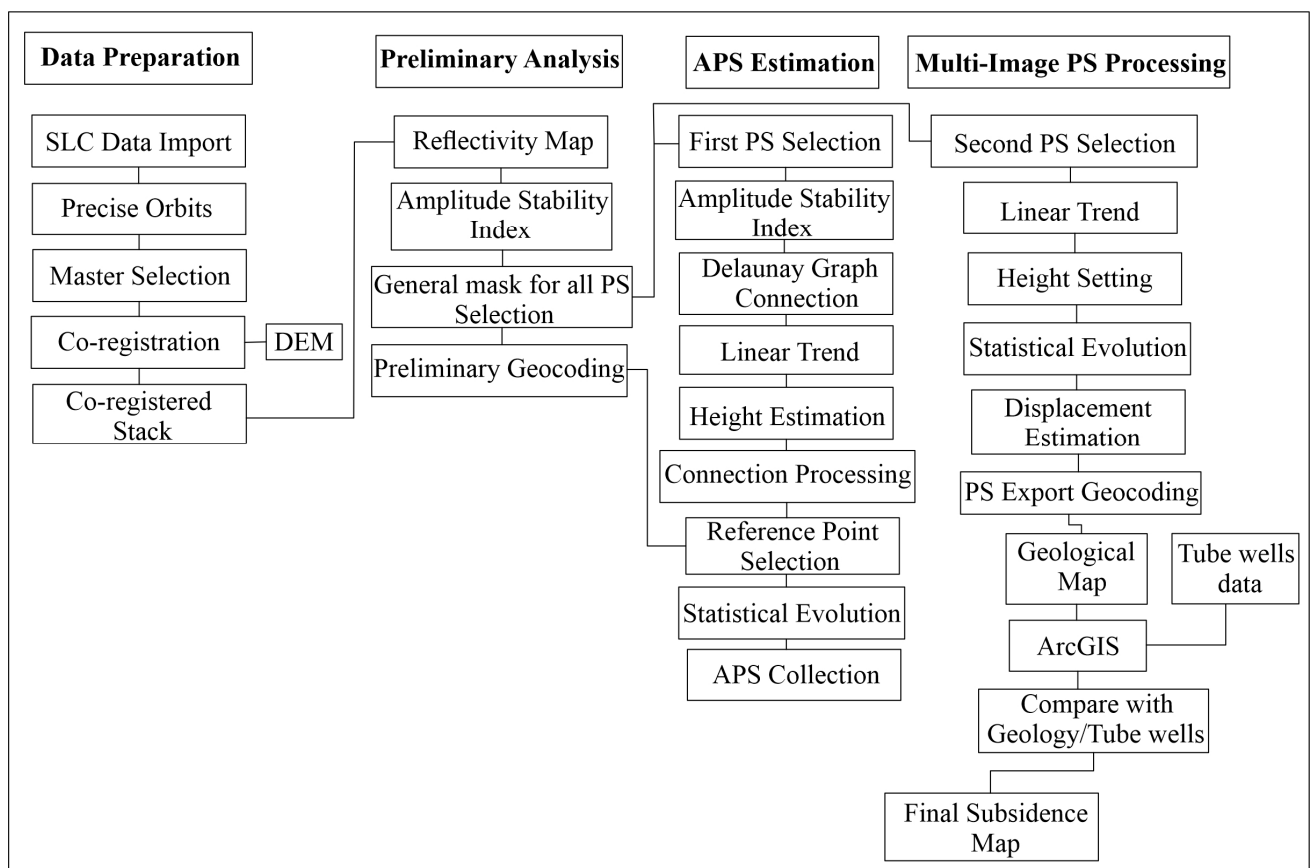


**Figure 4.** Data processing steps in methodology.

Other parameters such as the atmospheric phase screen (APS), track errors, and further considerations were estimated and eliminated. After that, the phase constancy was assessed. Absolute amplitude levels were essentially unconcerned about causing manipulation disturbances [71]. Consequently, it was projected that the pixels would have similar amplitudes and decreased phase distributions for these acquisitions. The Amplitude Stability Index (ASI) chooses PS in the Sarproz software procedure. Different atmospheric phase delays affect SAR images throughout the collection, and signal disruptions are common, such as radar signals impacted by aerosol fragments. The atmospheric phase screen is computed using several spatial–temporal filtrations [72]. At this step, the results of the atmospheric phase screen are eliminated, and the advanced stages are used to determine topographic height effects and linear displacement velocities.

Our study chose PSs based on ASI values greater than 0.6. This constraint parameter estimate is satisfied by permitting just a restricted amount of PS points, which is required to compute the correct atmospheric phase screen. Regarding the sequence of the first PS, a reference network must be built by linking PSs using Delaunay triangulation at this stage. The derived linear model (linear displacement velocities and residual height) is removed, and APS is evaluated using an inverse network from the phase residual. Defining a single point of reference and estimating the object's velocity here is also necessary. PS-InSAR relies

on a stable reference point to calculate relative velocity in respect to that point. As a result, special care must be used while choosing reference points for a combined PS-InSAR study from distinct orbits. Following APS and graph inversion deletion, the temporal coherence of PS was evaluated to test APS stability, producing an appropriate result with a coherence of more than 0.70 (Figure 6).

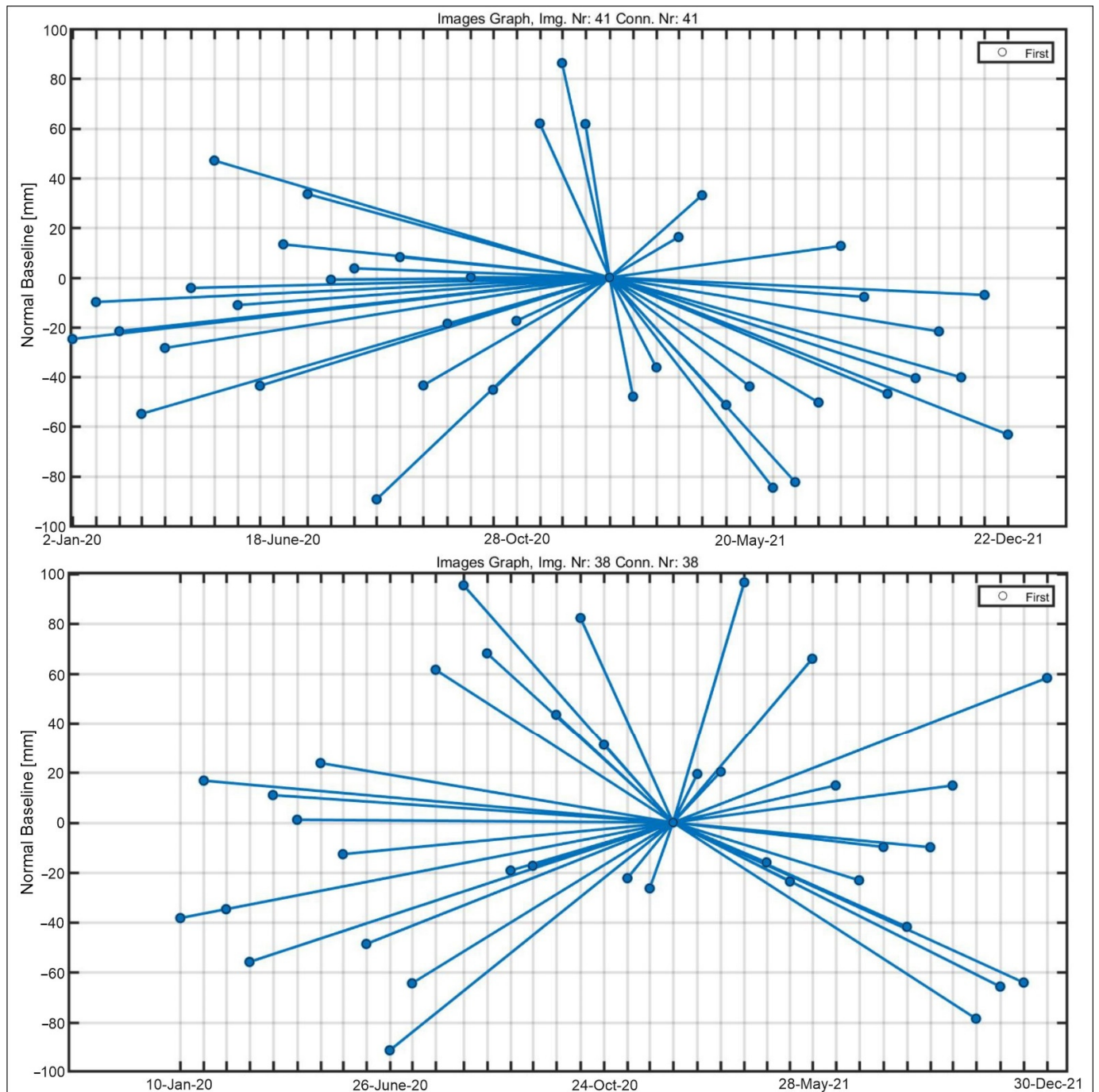
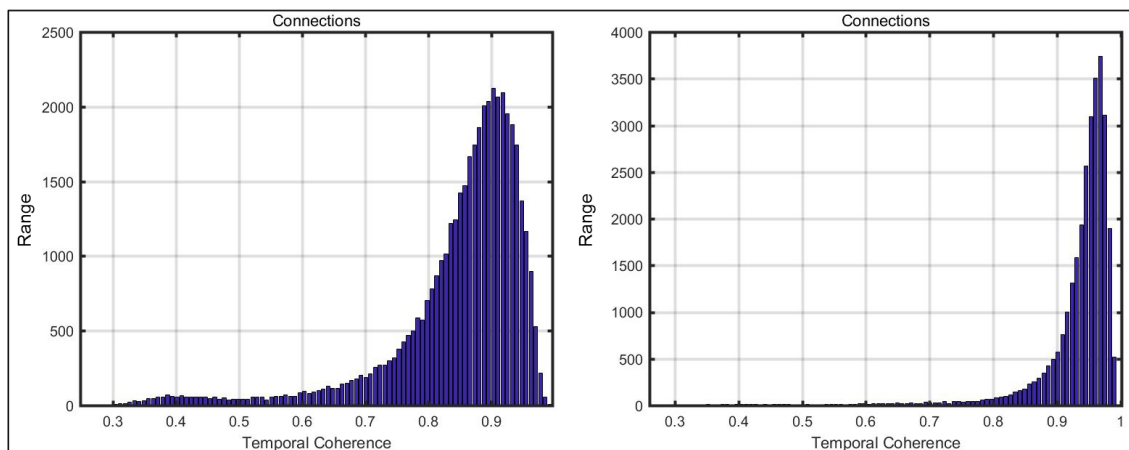


Figure 5. Star graphs showing the temporal/perpendicular baseline dispersion of data.



**Figure 6.** The graphs between the temporal coherence and connections for descending track (right side) and ascending track (left side) data.

In the Multi-Image Sparse Point (MISP) processing step, the second-order PS points were selected.  $ASI > 0.6$  criteria were applied at this phase to obtain thicker PS points. The same criteria and reference points used to calculate the APS estimate were used to remove APS. Finally, Persistent Scatterer points were geocoded and plotted on Google Earth, and only persistent scatterer points with a coherence of 0.70 or higher were included in the subsidence map [71].

Finally, the displacement zones were transformed into an exterior reference framework, i.e., geographical coordinates. The land subsidence and geology maps were overlaid and imported into a Geographic Information System (GIS) for additional analysis. The GIS investigation comprised merging PS-InSAR results with geology [29] and tube wells locations [73] to assess and validate the detected subsidence zones, which were then compared to Lahore's geological environment. These layers were used to assess the geological formations of the research area and their relationship to PS-InSAR projected subsidence.

### 3. Results

We used PS-InSAR integrated into Sarproz software for deformation monitoring in the area. Various stability thresholds highlight stable locations in green (from  $-20$  to  $-40$  mm/yr). PS-InSAR calculates and identifies movement in the region using a reference point; hence, a persistent point is selected as a reference point to correlate with the movement of other sites in the region. Temporal coherence must be adequate for further assessment when utilizing this approach. PS points with a temporal coherence  $> 0.70$  were considered dependable, with a decreased chance of error.

The use of PS points to measure motion along the line of sight (LOS) revealed that movement away from the sensor was small, as illustrated in red. Figure 7 presents more stable sites in the research region with less fluctuation (light blue to blue colors in Figure 7). Sites with considerable movement in comparison to the blue dots but smaller movements are labeled yellow and orange, respectively. Subsidence in Lahore has been estimated to fluctuate between  $-80$  and  $-25$  mm/year (Figure 7). According to the scatter plots, statistics show that Lahore city experienced severe subsidence.

The subsidence map obtained from both descending (track 34) and ascending (track 100) indicated a substantial number of PS sites in the studied area over the analysis period (Figure 8). The study area displays the ascending and descending scatter plots section on Google Earth. Figure 8 depicts a dense points cloud in the study location; the observations in both the ascending and descending directions reveal that the maximum area is steady (shown in green), primarily upland. The color ramp reflects the stability and movement of the PS points (green = low, yellow = constant, red = high).

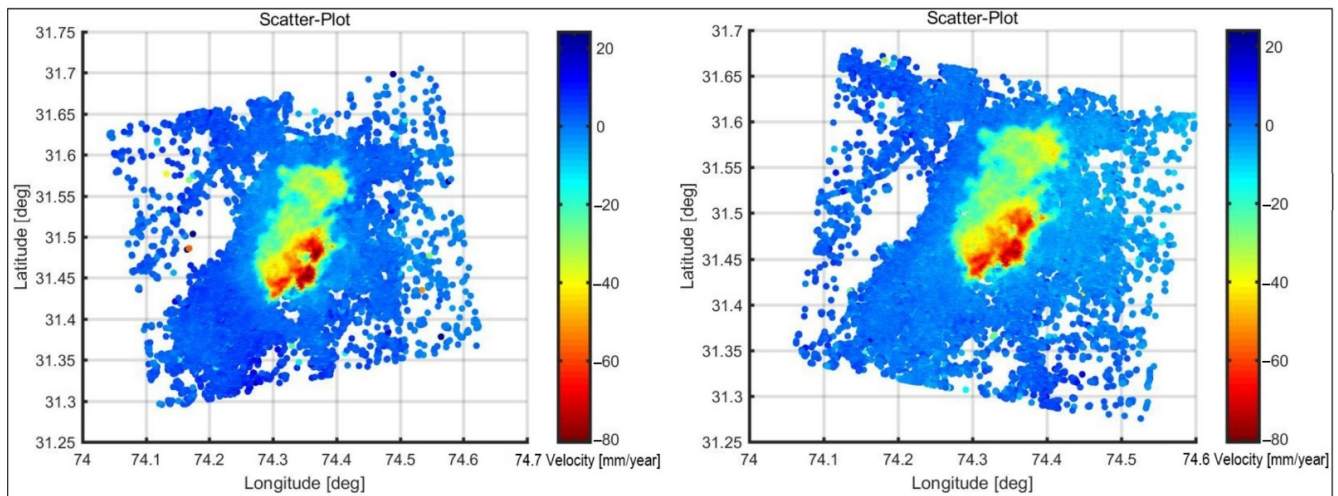


Figure 7. The scatter plots are ascending (left) and descending (right) (2020–2021).

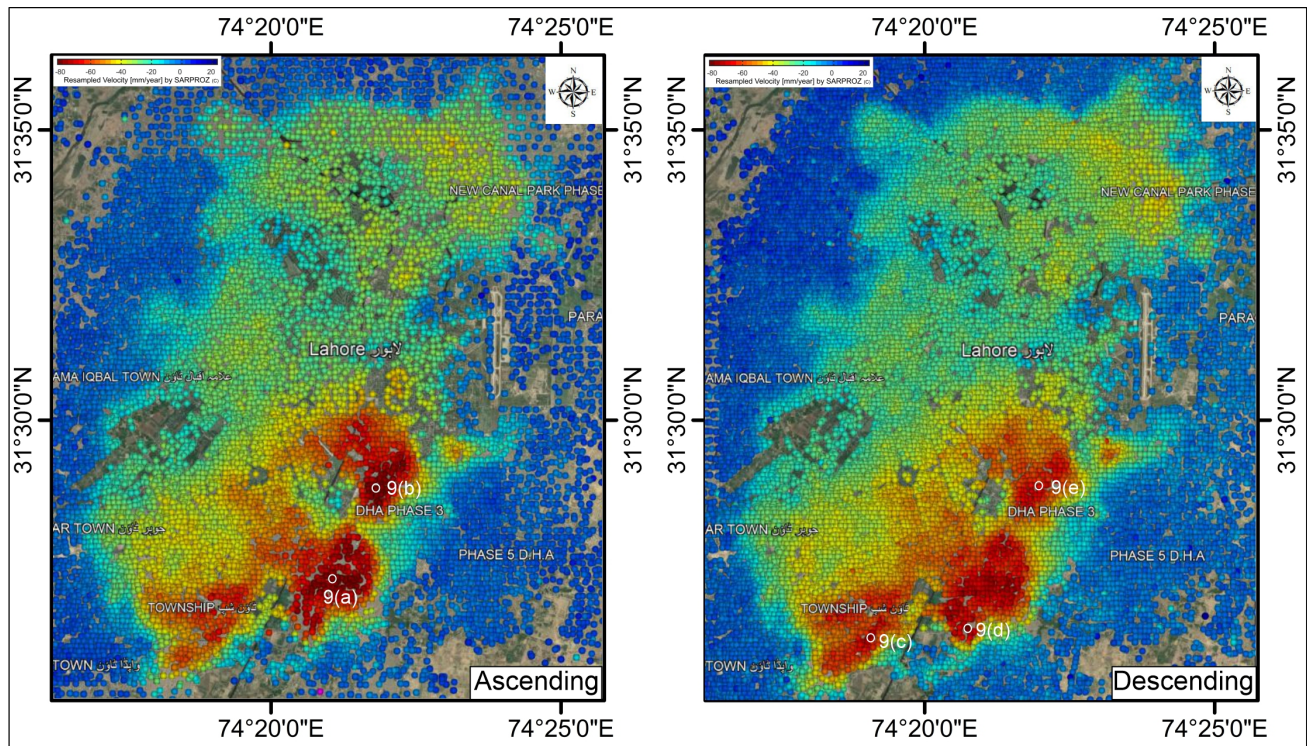
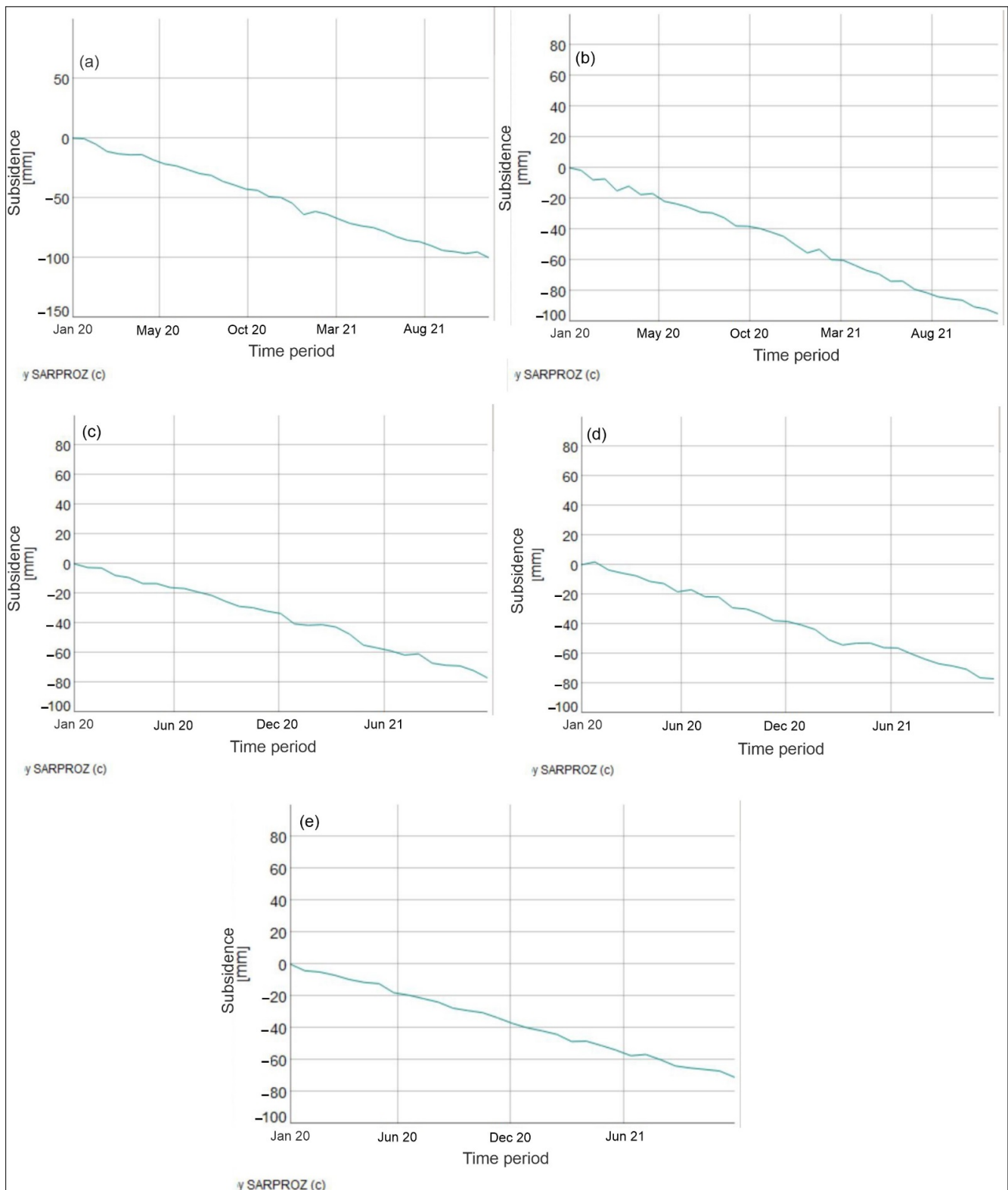


Figure 8. Ground subsidence in the study region from the Ascending path (a,b) and Descending path (c–e).

Five PS sites (a–d and e) from the subsidence area were selected from the research area’s ascending and descending results (Figure 9). In this scenario, the PS points depict the relative movement and stability in contrast to the surroundings. Subsidence analyses and these five PS sites are depicted in Figure 8.



**Figure 9.** PS points are chosen in ascending track (a,b) and descending track (c–e).

The red color delimits the subsidence area on the maps (Figure 8). The collected data show changes in ground movement from place to place during the investigation. In the research region, five points were chosen within the ascending (a,b) and descending (c–e) results (Figure 8). All the points are in the subsidence area and are plotted in Figure 9. The ascending a and b points, where LOS displacement reached  $-101$  mm and  $-96$  mm

during the study period. During the research duration, LOS displacement reached  $-77$  mm,  $-80$  mm, and  $-72$  mm in descending points c, d, and e.

Subsidence was examined along with these five PS sites, and the results show variations in subsidence from 2020 to 2021. The visual depictions of these five points are shown in Figure 9. The plots clearly show that points b and d have experienced significant subsidence over the research period.

The final subsidence map also examined the north to south subsidence pattern (x-axis has PS points, y-axis has subsidence) (Figure 10). The subsidence profile in Figure 11 demonstrates that subsidence was lower ( $-33$  mm) in the northern part of the city and increased ( $-81$  mm) towards the center. The ground subsidence decreases ( $-10$  mm, etc.) towards the southern part of the city but is only slightly less than in the northernmost point ( $-33$  mm) (Figure 11).

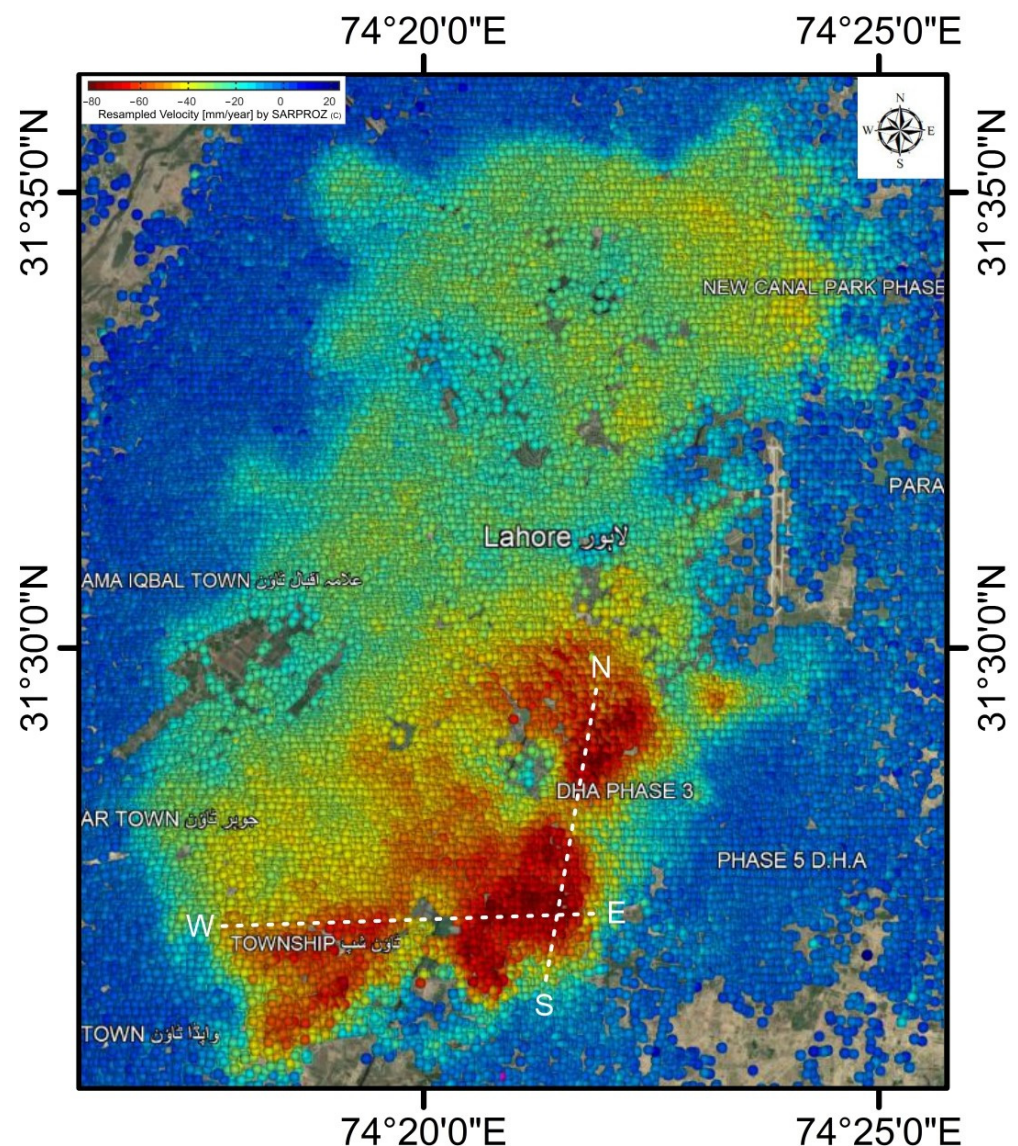
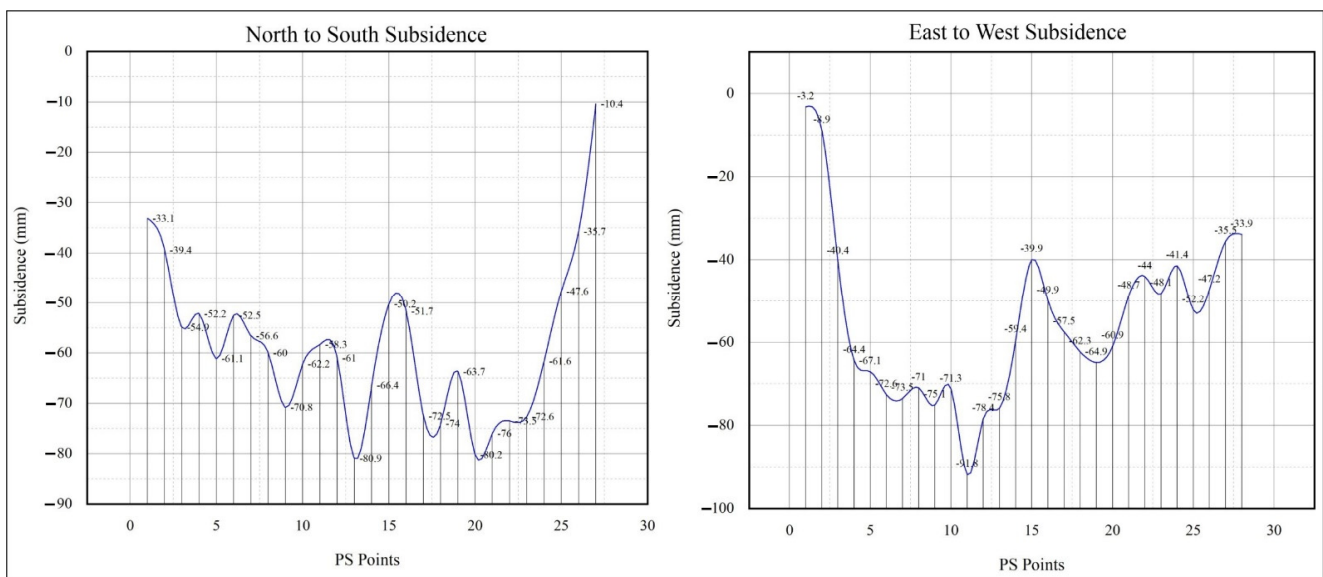


Figure 10. North to south and east to west subsidence profiles.



**Figure 11.** North to south and east to west subsidence graphs.

An east to west subsidence profile was obtained by plotting in the research area to evaluate the east–west subsidence pattern (x-axis has PS points, y-axis has subsidence) (Figure 10). According to this profile, the subsidence is lower (−3 mm, −9 mm, etc.) in the city’s eastern part (Figure 11). The central part of Lahore city has undergone considerable subsidence, reaching almost −92 mm (Figure 11), while the western part of the city has undergone smaller subsidence (−34 mm). This monitoring demonstrates that subsidence will be visible in the center of Lahore city between 2020 and 2021.

#### 4. Discussion

This study found that various elements are responsible for ground subsidence in Pakistan’s largest metropolis, Lahore. These are briefly described in the following.

##### 4.1. Subsurface Geology

The research objective is to examine the state of land subsidence in Lahore. High deformation areas are located in the study region’s center, which is Punjab’s economic and commercial hub. The surface deformation map supports the initial theory since places with significant urban activity exhibit higher deformation, whereas the land is stable moving out from the central part. Uplift can also be observed in near aquatic environments and areas with stronger refills.

Most of Lahore’s city was discovered to have developed on alluvium deposits [74]. The alluvium comprises sand, silt, and clay [75]. The Persistent Scatterer points overlaid on a geological map of Lahore city are seen in Figure 12. The ability of soil to consolidate has been identified as a primary source of liquefaction globally [76]. Most of the city’s buildings, including the military college, the institutions, and other commercial and residential structures, are built on quaternary alluvium. The study region is located in the Punjab Plain, and no significant earthquakes were recorded in the area throughout the investigation period.

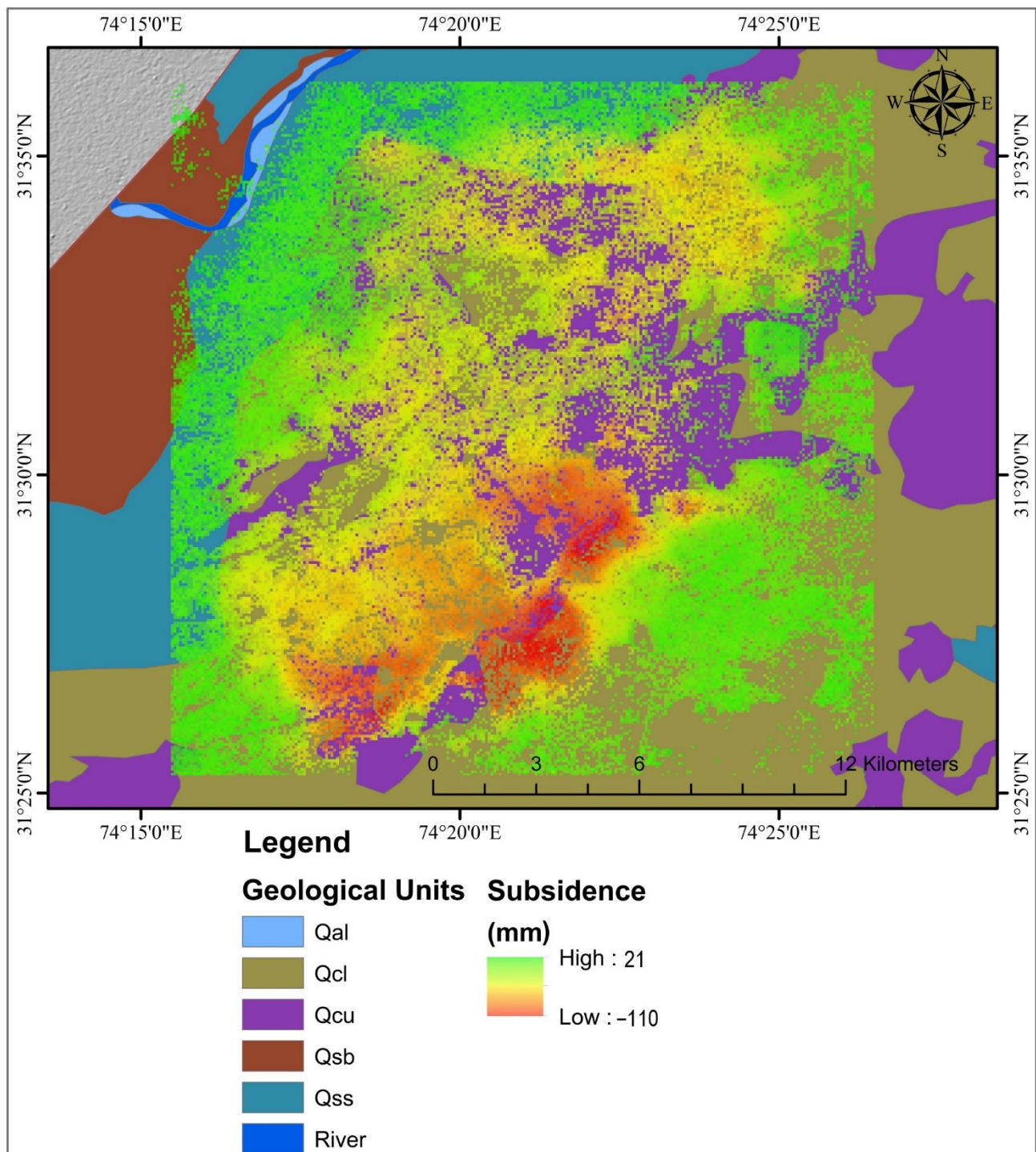


**Figure 12.** Subsidence on the geological map: Qal: recent deposit of Ravi River; Qcl: brown silt, clay, and sand; Qcu: meander-belt of deposit; Qsb: meander-belt of deposit of Ravi River; Qss: younger flood plain deposit; river.

#### 4.2. Precipitation

According to the data, the subsidence occurred primarily in quaternary alluvium (brown silt, clay and sand, and meander-belt deposit). Water precipitation into the subsurface, which penetrates the subsurface layers and induces infrastructure stresses, is most likely to produce subsidence in the investigated area. To confirm the subsidence in the study area, we examined the temporal association between subsidence at the examined

PS locations, namely a, b, c, d, and e and the yearly average precipitation (Figure 13). The precipitation data (Pakistan Metrological Department) in Lahore city indicated a substantial relationship with subsidence (Figure 13). The seasonal fluctuation in groundwater, primarily during monsoon rainfall (July and August), explains the reason for the area's subsidence. Monsoon rainfall recharges aquifers, stabilizing subsurface water and discharging the subsidence mechanism. This clearly shows the mechanism and subsidence reasons in the studied region.

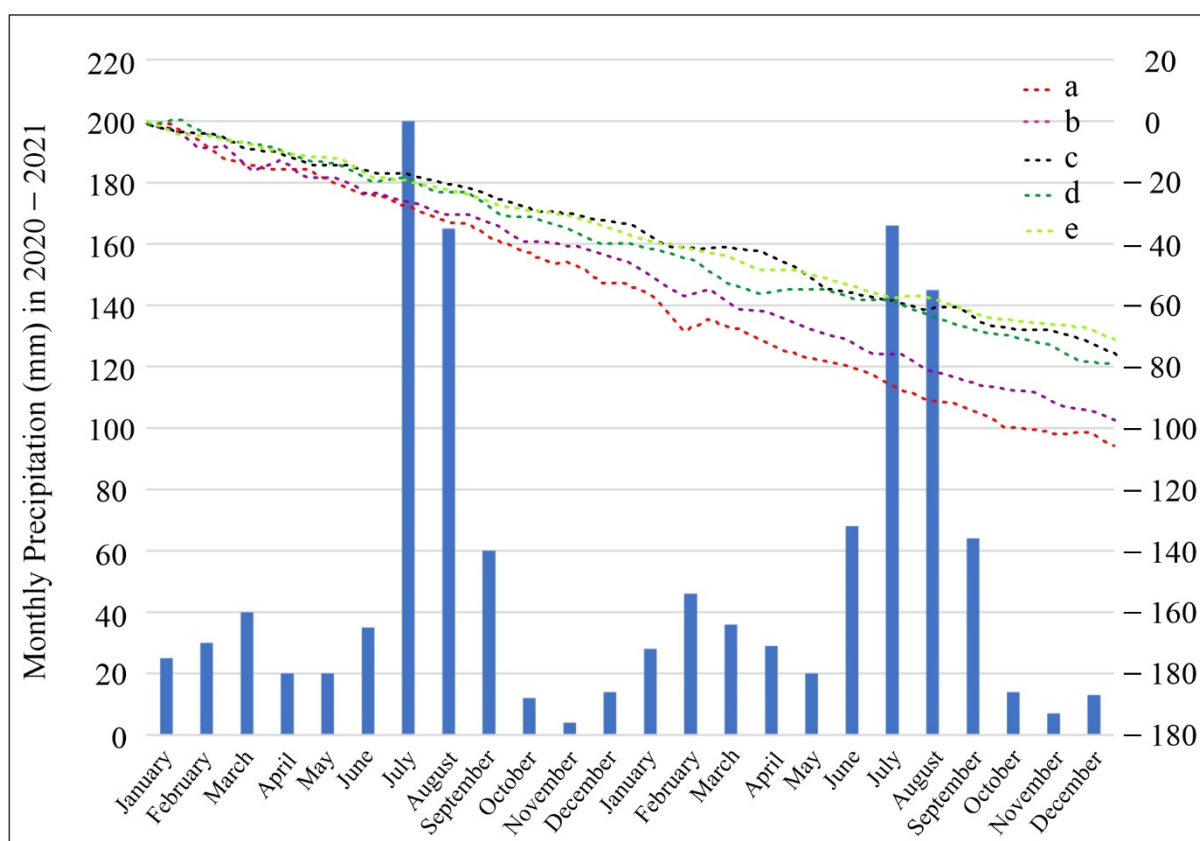


**Figure 13.** PS points from ascending track (a,b) and descending track (c–e) versus precipitation.

Furthermore, the relationship between subsidence and rainfall has been reported in [9,60], and excessive precipitation disrupts the balance of underground aquifers. This quantity of precipitation and other causative variables may affect subsidence. The high monsoon precipitation in the study region has previously been documented [77]. The saturation of the subsurface layers is caused by subsurface aquifer refilling, and a significant relationship between subsidence in the research area with rainfall has already been described [77].

#### 4.3. Groundwater Extraction

Groundwater removal is, without uncertainty, the most common cause of land subsidence worldwide [78,79]. Greater substantial groundwater extraction and groundwater reserves pressure have the potential to induce land subsidence since increased water removal creates a breach in the subsurface fluid that sustains the earth's surface equilibrium. The issue is exacerbated in dry locations where accessible surface water is needed, while environmental variations and other human causes raise groundwater pressure [80]. There is a water crisis in Lahore, Pakistan, and tube wells and bore wells are the principal source of regular water use [81]. Water usage has increased due to unplanned population development in large cities, and most homes have constructed a bore-well to suit their needs. Furthermore, this city is based in various commercial and state industries, such as those

in the chemical and agricultural sectors. These industries, for example, have substantial demand for groundwater use.

Groundwater data obtained from local authorities included the locations of government-owned water wells. Figure 14 shows that the most significant number of wells are situated in areas with the most significant amount of land deformation. According to the findings (Figures 10 and 11), ground subsidence is more common in the city center. One of the potential reasons is that excessive groundwater extraction from the tube well leads to land subsidence [73]. Fluctuations in fluid pressure in the subsurface layers due to excessive groundwater extraction cause the ground surface compaction [73]. The government plans to build wells to help the urban community with a bigger population size. Most wells in the higher subsidence zones have decreased water levels, whereas tube wells outside the deformation zones have higher water levels. The groundwater level dropped significantly from 48 to 59 m in 2020 to 2021. The population increased from 8.7 to 13.0 million in the last 10 years. In 2020, the population was 12.60 million, while in 2021 the population was 13.09 million, as shown in Figure 15. Lahore's daily water consumption is 480 million cubic gallons. In 2016, daily average water pumping by WASA (Water and Sanitation Agency) was around 540 million gallon per day, which means around 50 gallons per person per day. At present the daily average pumping by WASA through tube-wells increased to 750 million gallons per day, which means around 80 gallons per person per day.

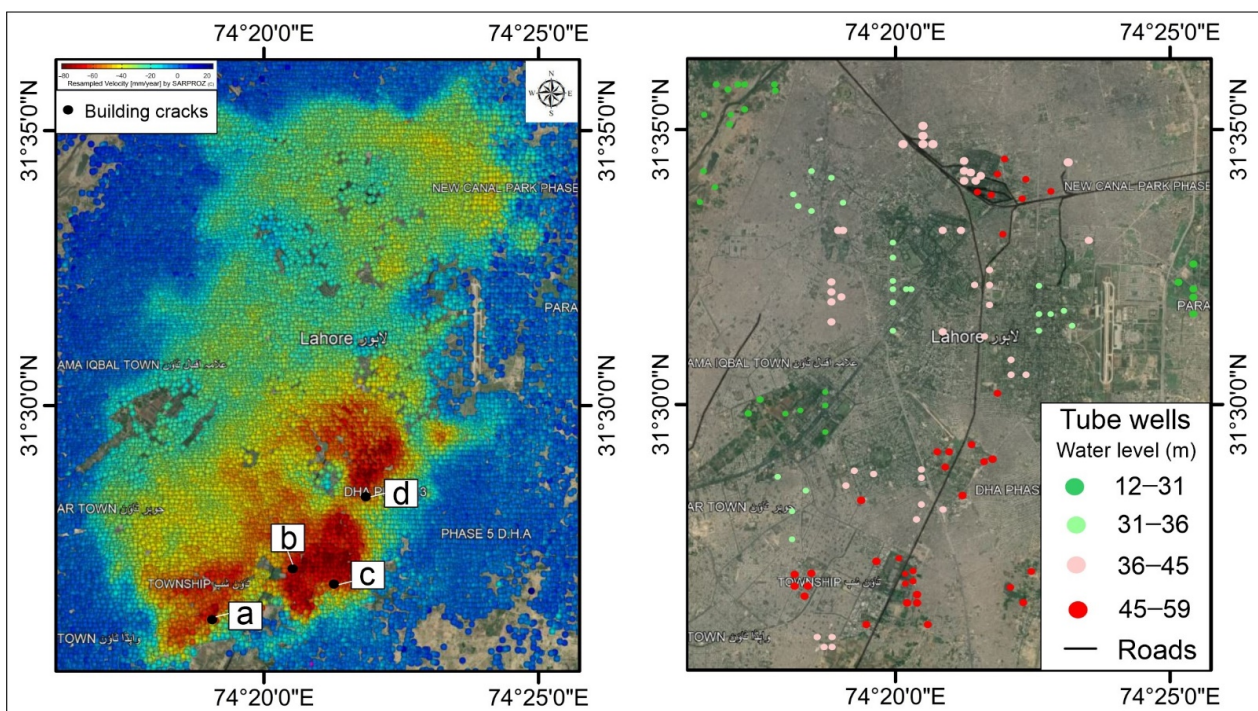


**Figure 14.** Tube well location map.

According to previous research, the authors believe that water extraction is the principal cause of subsidence, with these phenomena linked to soft clay soils [82–84]. Seasonal effects have been reported [82,85], which may be connected to hydrogeological variables and fluctuations in groundwater levels. One of the likely reasons for subsidence in the studied region is groundwater removal for commercial and household intents [73,86]. According to the previous study, excessive groundwater promotes ground instability [24,30,60,87,88].

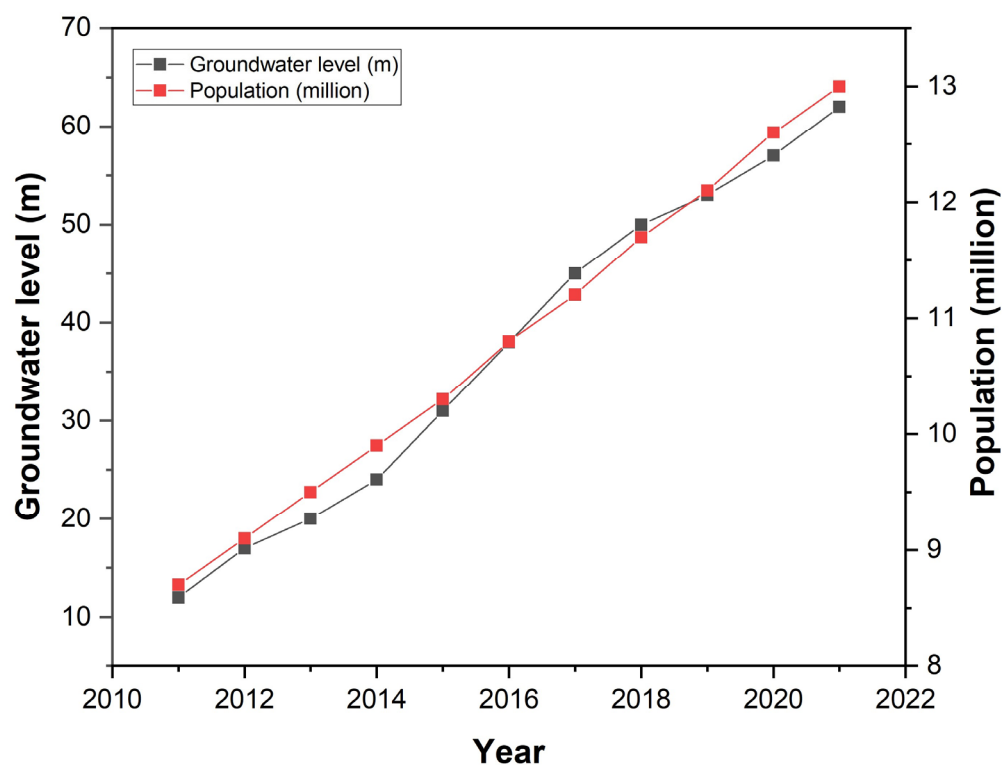


Figure 15. Change in groundwater level with increase in population.

Figure 14 depicts the deformation of the research area, and it can be observed that different portions of the city subside at different rates. Still, the large subsidence zones undergo considerable population increase and are the place of transportation and critical infrastructure sectors. When it comes to Pakistan's position, it has often been defined by its geographical configuration. It is the country where most people reside in places with the greatest commercial potential. Pakistan is urbanizing at the fastest rate in South Asia, with an annual rate of 3%. Metropolitan regions are facing rapid urbanization, with the number of residents in Karachi alone increasing by 80 percent between 2000 and 2010, the most significant increase of any district in the world [89]. Between 1999 and 2021, the urban area of Lahore city more than doubled [90]. A two-year PS-InSAR calculation revealed soil subsidence in regions with considerable groundwater abstraction and economic and urban activity.

Similar to previous studies [73], this was seen during field inspection for this research. As a result, we may argue that large-scale groundwater removal has increased in residential and industrial areas, which may be one reason for ground subsidence in Lahore. As a result, there have been a few cases of building collapse and fissures in the area (<https://www.bbc.com/news/world-asia-34720251> (accessed on 22 May 2022)). Figure 16 shows wall cracks in local houses, identified from field photos during the investigated period. The cracks found in local houses are attributed to subsidence in the study area. The images were taken throughout the rainy season (Figure 17). During rainy periods, water saturation on streets and roads was caused by unauthorized buildings and overgrown settlements [91]. Various streams flow from the surrounding area into the relatively large basin, where drainage blockages enable water to penetrate the subsoil [91]. According to the findings, subsidence in the research region is mostly caused by quaternary alluvium deposition layers, which are associated with the burden of infrastructures and are accountable for subsidence.



Figure 16. Building cracks due to ground subsidence in various places in Lahore City.



Figure 17. Water on the roads in Lahore City during rain.

#### 4.4. Uncertainties

At various spatiotemporal scales, several human and natural processes contribute to ground subsidence [53]. However, establishing the relevance of each aspect necessitates multiple sources of in-situ data that were not obtainable for this technique. We only examined subsurface deposit types and observed an intriguing relationship between them and higher surface deforming zones.

The low spatial resolution of the PS-InSAR study made identifying validation pairings challenging. As a result, it was difficult to determine which part of a structure was the main reflector. Furthermore, the PS points were georeferenced to the earth's surface, despite the fact that structures are three-dimensional, and satellites see the globe from all aspects. These factors must be taken into account while studying the PS points on the buildings. Due to the relatively low spatial resolution of C-band Sentinel-1 data, the geocoding of the SAR data sets was also a source of uncertainty.

Overall, the use of InSAR for monitoring subsidence has proven to be a promising technology. Denser acquisition plans and high pixel DEM will enhance detecting accuracy by minimizing noise in the time series and velocity field [92]. Land truthing in the study region is difficult because most structures are civilian assets, and landowners may refuse accessibility due to the danger of asset value loss. However, radar interferometry detects subsidence across wide distances, making it easier to locate places where comprehensive ground truthing is desired.

Despite these uncertainties, our findings correctly identified subsidence occurrences in the study region after confirming them with soil consolidation, tubewell data, and subsurface geology in the research area. However, various alternative procedures such as Quasi-PS and SBAS techniques with accurate levelling in the research region can considerably enhance it. Finally, well log data and geotechnical investigation will be required in the future to determine a more accurate subsidence rate.

#### 5. Conclusions

Globally, urbanization and groundwater extraction are key drivers of land subsidence. Lahore is a megacity undergoing ongoing population expansion and development, even though groundwater removal is relatively high.

In this work, we detected ground subsidence in Lahore from 2020 to 2021, demonstrating the ability of PS-InSAR to check time series subsidence. In the research area, the cumulative deformation varied from  $-110$  mm to  $21$  mm from 2019 to 2020. The data analysis results showed significant subsidence in the city center over the research duration. The most apparent explanations have been recent rapid population growth and increasing demand for regular water usage (industry and home) and groundwater removal. The key approach components have been extensively defined, and various noise and inaccuracy reduction approaches have been implemented throughout the procedure. Various causative variables have been investigated, including groundwater removal, soil consolidation, subsurface geology, and so on. The subsidence maps in the research region indicate that Lahore is experiencing significant ground subsidence. The outcomes also propose that subsidence is higher in the city center, although substantially lower in the research region's outskirts.

PS-InSAR is an extremely useful technique for monitoring urban structure collapse, land subsidence, and other similar phenomena. Our findings successfully revealed subsidence phenomena in the study area; however, they may be enhanced by in situ data assessment and different methodologies such as the SBAS technique or Quasi-PS. It is also suggested that multi-scale studies be conducted to thoroughly investigate subsidence in the future and avoid substantial impact in this region.

**Author Contributions:** Conceptualization, M.A.H.; methodology, M.A.H. and Y.Z.; software, M.A.H. and Y.Z.; validation, M.S.; formal analysis, J.M.; investigation, I.A.; resources, Z.C.; data curation, J.K.; writing—original draft preparation, M.A.H.; writing—review and editing, J.M. and A.A.; visualiza-

tion, M.S.; supervision, Z.C.; project administration, Z.C.; funding acquisition, Z.C. All authors have read and agreed to the published version of the manuscript.

**Funding:** This research was funded by the National Natural Science Foundation of China (No. 41871305); National key R & D program of China (No. 2017YFC0602204); Fundamental Research Funds for the Central Universities, China University of Geosciences (Wuhan) (No. CUGQY1945); Opening Fund of Key Laboratory of Geological Survey and Evaluation of Ministry of Education; and Fundamental Research Funds for the Central Universities (No. GLAB2019ZR02).

**Data Availability Statement:** The data presented in the study are available on request from the first and corresponding author. The data are not publicly available due to the thesis that is being prepared from these data.

**Conflicts of Interest:** The authors declare no conflict of interest.

## References

- Zhou, L.; Guo, J.; Hu, J.; Li, J.; Xu, Y.; Pan, Y.; Shi, M. Wuhan surface subsidence analysis in 2015–2016 based on Sentinel-1A data by SBAS-InSAR. *Remote Sens.* **2017**, *9*, 982. [[CrossRef](#)]
- Hu, B.; Zhou, J.; Wang, J.; Chen, Z.; Wang, D.; Xu, S. Risk assessment of land subsidence at Tianjin coastal area in China. *Environ. Earth Sci.* **2009**, *59*, 269–276. [[CrossRef](#)]
- Du, Z.; Ge, L.; Ng, A.H.-M.; Xiaojing, L.; Li, L. Mapping land subsidence over the eastern Beijing city using satellite radar interferometry. *Int. J. Digit. Earth* **2018**, *11*, 504–519. [[CrossRef](#)]
- Chen, M.; Tomás, R.; Li, Z.; Motagh, M.; Li, T.; Hu, L.; Gong, H.; Li, X.; Yu, J.; Gong, X. Imaging land subsidence induced by groundwater extraction in Beijing (China) using satellite radar interferometry. *Remote Sens.* **2016**, *8*, 468. [[CrossRef](#)]
- Zhang, T.; Shen, W.-B.; Wu, W.; Zhang, B.; Pan, Y. Recent surface deformation in the Tianjin area revealed by Sentinel-1A data. *Remote Sens.* **2019**, *11*, 130. [[CrossRef](#)]
- Chen, J.; Wu, J.; Zhang, L.; Zou, J.; Liu, G.; Zhang, R.; Yu, B. Deformation trend extraction based on multi-temporal InSAR in Shanghai. *Remote Sens.* **2013**, *5*, 1774–1786. [[CrossRef](#)]
- Zhu, W.; Li, W.-L.; Zhang, Q.; Yang, Y.; Zhang, Y.; Qu, W.; Wang, C.-S. A decade of ground deformation in Kunming (China) revealed by multi-temporal synthetic aperture radar interferometry (InSAR) technique. *Sensors* **2019**, *19*, 4425. [[CrossRef](#)] [[PubMed](#)]
- Liu, X.; Xing, X.; Wen, D.; Chen, L.; Yuan, Z.; Liu, B.; Tan, J. Mining-induced time-series deformation investigation based on SBAS-InSAR technique: A case study of drilling water solution rock salt mine. *Sensors* **2019**, *19*, 5511. [[CrossRef](#)] [[PubMed](#)]
- Zhang, Y.; Liu, Y.; Jin, M.; Jing, Y.; Liu, Y.; Liu, Y.; Sun, W.; Wei, J.; Chen, Y. Monitoring land subsidence in Wuhan city (China) using the SBAS-InSAR method with radarsat-2 imagery data. *Sensors* **2019**, *19*, 743. [[CrossRef](#)]
- Liu, G.; Luo, X.; Chen, Q.; Huang, D.; Ding, X. Detecting land subsidence in Shanghai by PS-networking SAR interferometry. *Sensors* **2008**, *8*, 4725–4741. [[CrossRef](#)]
- Ma, J.; Xia, D.; Guo, H.; Wang, Y.; Niu, X.; Liu, Z.; Jiang, S. Metaheuristic-based support vector regression for landslide displacement prediction: A comparative study. *Landslides* **2022**, *19*, 1–23. [[CrossRef](#)]
- Kumar, S.; Kumar, D.; Donta, P.K.; Amgoth, T. Land subsidence prediction using recurrent neural networks. *Stoch. Environ. Res. Risk Assess.* **2022**, *36*, 373–388. [[CrossRef](#)]
- Subhanil, G.; Govil, H. Estimating the seasonal relationship between land surface temperature and normalized difference bareness index using Landsat data series. *Int. J. Eng. Geosci.* **2020**, *7*, 9–16.
- Orhan, O.; Oliver-Cabrera, T.; Wdowinski, S.; Yalvac, S.; Yakar, M. Land subsidence and its relations with sinkhole activity in Karapınar region, Turkey: A multi-sensor InSAR time series study. *Sensors* **2021**, *21*, 774. [[CrossRef](#)]
- Ahady, A.B.; Kaplan, G. Classification comparison of Landsat-8 and Sentinel-2 data in Google Earth Engine, study case of the city of Kabul. *Int. J. Eng. Geosci.* **2022**, *7*, 24–31. [[CrossRef](#)]
- Karimzadeh, S.; Matsuoka, M. Remote Sensing X-Band SAR Data for land subsidence and pavement monitoring. *Sensors* **2020**, *20*, 4751. [[CrossRef](#)] [[PubMed](#)]
- Mohebbi Tafreshi, G.; Nakhaei, M.; Lak, R. A GIS-based comparative study of hybrid fuzzy-gene expression programming and hybrid fuzzy-artificial neural network for land subsidence susceptibility modeling. *Stoch. Environ. Res. Risk Assess.* **2020**, *34*, 1059–1087. [[CrossRef](#)]
- Arabameri, A.; Santosh, M.; Rezaie, F.; Saha, S.; Coastache, R.; Roy, J.; Mukherjee, K.; Tiefenbacher, J. Application of novel ensemble models and k-fold CV approaches for Land subsidence susceptibility modelling. *Stoch. Environ. Res. Risk Assess.* **2022**, *36*, 201–223. [[CrossRef](#)]
- Ezquerro, P.; Del Soldato, M.; Solari, L.; Tomás, R.; Raspini, F.; Ceccatelli, M.; Fernández-Merodo, J.A.; Casagli, N.; Herrera, G. Vulnerability assessment of buildings due to land subsidence using InSAR data in the ancient historical city of Pistoia (Italy). *Sensors* **2020**, *20*, 2749. [[CrossRef](#)]

20. Stramondo, S.; Bozzano, F.; Marra, F.; Wegmuller, U.; Cinti, F.; Moro, M.; Saroli, M. Subsidence induced by urbanisation in the city of Rome detected by advanced InSAR technique and geotechnical investigations. *Remote Sens. Environ.* **2008**, *112*, 3160–3172. [[CrossRef](#)]
21. Pratesi, F.; Tapete, D.; Del Ventisette, C.; Moretti, S. Mapping interactions between geology, subsurface resource exploitation and urban development in transforming cities using InSAR Persistent Scatterers: Two decades of change in Florence, Italy. *Appl. Geogr.* **2016**, *77*, 20–37. [[CrossRef](#)]
22. Solari, L.; Ciampalini, A.; Raspini, F.; Bianchini, S.; Moretti, S. PSInSAR analysis in the Pisa urban area (Italy): A case study of subsidence related to stratigraphical factors and urbanization. *Remote Sens.* **2016**, *8*, 120. [[CrossRef](#)]
23. Nonaka, T.; Asaka, T.; Iwashita, K.; Ogushi, F. Evaluation of the trend of deformation around the Kanto Region estimated using the time series of PALSAR-2 Data. *Sensors* **2020**, *20*, 339. [[CrossRef](#)] [[PubMed](#)]
24. Zheng, M.; Fukuyama, K.; Sanga-Ngoie, K. Application of InSAR and GIS techniques to ground subsidence assessment in the Nobi Plain, Central Japan. *Sensors* **2014**, *14*, 492–509. [[CrossRef](#)]
25. Castellazzi, P.; Arroyo-Domínguez, N.; Martel, R.; Calderhead, A.I.; Normand, J.C.; Gárfias, J.; Rivera, A. Land subsidence in major cities of Central Mexico: Interpreting InSAR-derived land subsidence mapping with hydrogeological data. *Int. J. Appl. Earth Obs. Geoinf.* **2016**, *47*, 102–111. [[CrossRef](#)]
26. Chaussard, E.; Wdowinski, S.; Cabral-Cano, E.; Amelung, F. Land subsidence in central Mexico detected by ALOS InSAR time-series. *Remote Sens. Environ.* **2014**, *140*, 94–106. [[CrossRef](#)]
27. Ng, A.H.-M.; Ge, L.; Li, X.; Abidin, H.Z.; Andreas, H.; Zhang, K. Mapping land subsidence in Jakarta, Indonesia using persistent scatterer interferometry (PSI) technique with ALOS PALSAR. *Int. J. Appl. Earth Obs. Geoinf.* **2012**, *18*, 232–242. [[CrossRef](#)]
28. Chaussard, E.; Amelung, F.; Abidin, H.; Hong, S.-H. Sinking cities in Indonesia: ALOS PALSAR detects rapid subsidence due to groundwater and gas extraction. *Remote Sens. Environ.* **2013**, *128*, 150–161. [[CrossRef](#)]
29. Amin, G.; Shahzad, M.I.; Jaweria, S.; Zia, I. Measuring land deformation in a mega city Karachi-Pakistan with Sentinel SAR Interferometry. *Geocarto Int.* **2021**, *1*, 1–15. [[CrossRef](#)]
30. Khan, J.; Ren, X.; Hussain, M.A.; Jan, M.Q. Monitoring Land Subsidence Using PS-InSAR Technique in Rawalpindi and Islamabad, Pakistan. *Remote Sens.* **2022**, *14*, 3722. [[CrossRef](#)]
31. Shahzad, N.; Ding, X.; Wu, S.; Liang, H. Ground deformation and its causes in abbotabad city, pakistan from sentinel-1a data and mt-insar. *Remote Sens.* **2020**, *12*, 3442. [[CrossRef](#)]
32. Hussain, M.A.; Chen, Z.; Shoaib, M.; Shah, S.U.; Khan, J.; Ying, Z. Sentinel-1A for monitoring land subsidence of coastal city of Pakistan using Persistent Scatterers In-SAR technique. *Sci. Rep.* **2022**, *12*, 1–18.
33. Kaneko, S.; Toyota, T. Long-term urbanization and land subsidence in Asian Megacities: An indicators system approach. In *Groundwater and Subsurface Environments*; Springer: Berlin/Heidelberg, Germany, 2011; pp. 249–270.
34. Infante, D.; Di Martire, D.; Confuorto, P.; Tessitore, S.; Tòmas, R.; Calcaterra, D.; Ramondini, M. Assessment of building behavior in slow-moving landslide-affected areas through DInSAR data and structural analysis. *Eng. Struct.* **2019**, *199*, 109638. [[CrossRef](#)]
35. Peduto, D.; Pisciotta, G.; Nicodemo, G.; Arena, L.; Ferlisi, S.; Gullà, G.; Borrelli, L.; Fornaro, G.; Reale, D. A procedure for the analysis of building vulnerability to slow-moving landslides. In Proceedings of the 1st IMEKO International Workshop on Metrology for Geotechnics, Athena Srl, Benevento, Italy, 17–18 March 2016; pp. 248–254.
36. Shoaib, M.; Yang, W.; Liang, Y.; Rehman, G. Stability and deformation analysis of landslide under coupling effect of rainfall and reservoir drawdown. *Civ. Eng. J.* **2021**, *7*, 1098–1111. [[CrossRef](#)]
37. Talledo, D.A.; Miano, A.; Bonano, M.; Di Carlo, F.; Lanari, R.; Manunta, M.; Meda, A.; Mele, A.; Prota, A.; Saetta, A. Satellite radar interferometry: Potential and limitations for structural assessment and monitoring. *J. Build. Eng.* **2022**, *46*, 103756. [[CrossRef](#)]
38. Ma, J.; Xia, D.; Wang, Y.; Niu, X.; Jiang, S.; Liu, Z.; Guo, H. A comprehensive comparison among metaheuristics (MHs) for geohazard modeling using machine learning: Insights from a case study of landslide displacement prediction. *Eng. Appl. Artif. Intell.* **2022**, *114*, 105150. [[CrossRef](#)]
39. Ikuemonisan, F.E.; Ozebo, V.C. Characterisation and mapping of land subsidence based on geodetic observations in Lagos, Nigeria. *Geod. Geodyn.* **2020**, *11*, 151–162. [[CrossRef](#)]
40. Buzzanga, B.; Bekaert, D.P.; Hamlington, B.D.; Sangha, S.S. Toward sustained monitoring of subsidence at the coast using InSAR and GPS: An application in Hampton Roads, Virginia. *Geophys. Res. Lett.* **2020**, *47*, e2020GL090013. [[CrossRef](#)]
41. Da Lio, C.; Tosi, L. Land subsidence in the Friuli Venezia Giulia coastal plain, Italy: 1992–2010 results from SAR-based interferometry. *Sci. Total Environ.* **2018**, *633*, 752–764. [[CrossRef](#)]
42. Tzouvaras, M.; Kouhartsiouk, D.; Agapiou, A.; Danezis, C.; Hadjimitsis, D.G. The use of Sentinel-1 synthetic aperture radar (SAR) images and open-source software for cultural heritage: An example from Paphos area in Cyprus for mapping landscape changes after a 5.6 magnitude earthquake. *Remote Sens.* **2019**, *11*, 1766. [[CrossRef](#)]
43. Chen, B.; Gong, H.; Li, X.; Lei, K.; Gao, M.; Zhou, C.; Ke, Y. Spatial-temporal evolution patterns of land subsidence with different situation of space utilization. *Nat. Hazards* **2015**, *77*, 1765–1783. [[CrossRef](#)]
44. Hussain, M.A.; Chen, Z.; Zheng, Y.; Shoaib, M.; Shah, S.U.; Ali, N.; Afzal, Z. Landslide susceptibility mapping using machine learning algorithm validated by persistent scatterer In-SAR technique. *Sensors* **2022**, *22*, 3119. [[CrossRef](#)] [[PubMed](#)]
45. Manconi, A.; Kourkouli, P.; Caduff, R.; Strozzi, T.; Loew, S. Monitoring surface deformation over a failing rock slope with the ESA sentinels: Insights from Moosfluh instability, Swiss Alps. *Remote Sens.* **2018**, *10*, 672. [[CrossRef](#)]

46. Fiorentini, N.; Maboudi, M.; Leandri, P.; Losa, M. Can machine learning and PS-InSAR reliably stand in for road profilometric surveys? *Sensors* **2021**, *21*, 3377. [[CrossRef](#)] [[PubMed](#)]
47. Galve, J.P.; Castañeda, C.; Gutiérrez, F.; Herrera, G. Assessing sinkhole activity in the Ebro Valley mantled evaporite karst using advanced DInSAR. *Geomorphology* **2015**, *229*, 30–44. [[CrossRef](#)]
48. Tofani, V.; Raspini, F.; Catani, F.; Casagli, N. Persistent Scatterer Interferometry (PSI) technique for landslide characterization and monitoring. *Remote Sens.* **2013**, *5*, 1045–1065. [[CrossRef](#)]
49. Yang, Q.; Ke, Y.; Zhang, D.; Chen, B.; Gong, H.; Lv, M.; Zhu, L.; Li, X. Multi-scale analysis of the relationship between land subsidence and buildings: A case study in an eastern Beijing Urban Area using the PS-InSAR technique. *Remote Sens.* **2018**, *10*, 1006. [[CrossRef](#)]
50. Gao, M.; Gong, H.; Chen, B.; Zhou, C.; Chen, W.; Liang, Y.; Shi, M.; Si, Y. InSAR time-series investigation of long-term ground displacement at Beijing Capital International Airport, China. *Tectonophysics* **2016**, *691*, 271–281. [[CrossRef](#)]
51. Shi, L.; Gong, H.; Chen, B.; Zhou, C. Land Subsidence Prediction Induced by Multiple Factors Using Machine Learning Method. *Remote Sens.* **2020**, *12*, 4044. [[CrossRef](#)]
52. Beladam, O.; Balz, T.; Mohamadi, B.; Abdalhak, M. Using ps-insar with sentinel-1 images for deformation monitoring in northeast Algeria. *Geosciences* **2019**, *9*, 315. [[CrossRef](#)]
53. Milillo, P.; Giardina, G.; DeJong, M.J.; Perissin, D.; Milillo, G. Multi-temporal InSAR structural damage assessment: The London crossrail case study. *Remote Sens.* **2018**, *10*, 287. [[CrossRef](#)]
54. Agarwal, V.; Kumar, A.; L Gomes, R.; Marsh, S. Monitoring of ground movement and groundwater changes in London using InSAR and GRACE. *Appl. Sci.* **2020**, *10*, 8599. [[CrossRef](#)]
55. Khorrami, M.; Abrishami, S.; Maghsoudi, Y.; Alizadeh, B.; Perissin, D. Extreme subsidence in a populated city (Mashhad) detected by PSInSAR considering groundwater withdrawal and geotechnical properties. *Sci. Rep.* **2020**, *10*, 1–16. [[CrossRef](#)] [[PubMed](#)]
56. Khorrami, M.; Alizadeh, B.; Ghasemi Tousi, E.; Shakerian, M.; Maghsoudi, Y.; Rahgozar, P. How groundwater level fluctuations and geotechnical properties lead to asymmetric subsidence: A PSInSAR analysis of land deformation over a transit corridor in the Los Angeles metropolitan area. *Remote Sens.* **2019**, *11*, 377. [[CrossRef](#)]
57. Mateos, R.M.; Ezquerro, P.; Luque-Espinar, J.A.; Béjar-Pizarro, M.; Notti, D.; Azañón, J.M.; Montserrat, O.; Herrera, G.; Fernández-Chacón, F.; Peinado, T. Multiband PSInSAR and long-period monitoring of land subsidence in a strategic detrital aquifer (Vega de Granada, SE Spain): An approach to support management decisions. *J. Hydrol.* **2017**, *553*, 71–87. [[CrossRef](#)]
58. Cian, F.; Blasco, J.M.D.; Carrera, L. Sentinel-1 for monitoring land subsidence of coastal cities in Africa using PSInSAR: A methodology based on the integration of SNAP and StaMPS. *Geosciences* **2019**, *9*, 124. [[CrossRef](#)]
59. Grzempowski, P.; Badura, J.; Milczarek, W.; Blachowski, J.; Głowacki, T.; Zajac, M. Determination of the Long-Term Ground Surface Displacements Using a PSI Technique—Case Study on Wrocław (Poland). *Appl. Sci.* **2020**, *10*, 3343. [[CrossRef](#)]
60. Khan, R.; Li, H.; Afzal, Z.; Basir, M.; Arif, M.; Hassan, W. Monitoring Subsidence in Urban Area by PSInSAR: A Case Study of Abbottabad City, Northern Pakistan. *Remote Sens.* **2021**, *13*, 1651. [[CrossRef](#)]
61. Pepe, A.; Calò, F. A review of interferometric synthetic aperture RADAR (InSAR) multi-track approaches for the retrieval of Earth's surface displacements. *Appl. Sci.* **2017**, *7*, 1264. [[CrossRef](#)]
62. Zhou, C.; Lan, H.; Gong, H.; Zhang, Y.; Warner, T.A.; Clague, J.J.; Wu, Y. Reduced rate of land subsidence since 2016 in Beijing, China: Evidence from Tomo-PSInSAR using RadarSAT-2 and Sentinel-1 datasets. *Int. J. Remote Sens.* **2020**, *41*, 1259–1285. [[CrossRef](#)]
63. Duan, W.; Zhang, H.; Tang, Y.; Wang, C.; Zeng, X.; Wang, J. Land subsidence monitoring for Beijing-tianjin-hebei region using sentinel-1. In Proceedings of the 2019 SAR in Big Data Era (BIGSAR DATA), Beijing, China, 5–6 August 2019; pp. 1–4.
64. Kazmi, A.H.; Jan, M.Q. *Geology and Tectonics of Pakistan*; Graphic Publishers: Karachi, Pakistan, 1997.
65. Naeem, M.; Khan, K.; Rehman, S.; Iqbal, J. Environmental assessment of ground water quality of Lahore area, Punjab, Pakistan. *J. Appl. Sci.* **2007**, *7*, 41–46. [[CrossRef](#)]
66. Crosetto, M.; Devanthery, N.; Cuevas-González, M.; Monserrat, O.; Crippa, B. Exploitation of the full potential of PSI data for subsidence monitoring. *Proc. Int. Assoc. Hydrol. Sci.* **2015**, *372*, 311–314. [[CrossRef](#)]
67. Hussain, M.A.; Chen, Z.; Wang, R.; Shoaib, M. PS-InSAR-Based Validated Landslide Susceptibility Mapping along Karakorum Highway, Pakistan. *Remote Sens.* **2021**, *13*, 4129. [[CrossRef](#)]
68. Yagüe-Martínez, N.; Prats-Iraola, P.; Gonzalez, F.R.; Bric, R.; Shau, R.; Geudtner, D.; Eineder, M.; Bamler, R. Interferometric processing of Sentinel-1 TOPS data. *IEEE Trans. Geosci. Remote Sens.* **2016**, *54*, 2220–2234. [[CrossRef](#)]
69. Zhou, C.; Gong, H.; Zhang, Y.; Warner, T.A.; Wang, C. Spatiotemporal evolution of land subsidence in the Beijing plain 2003–2015 using persistent scatterer interferometry (PSI) with multi-source SAR data. *Remote Sens.* **2018**, *10*, 552. [[CrossRef](#)]
70. Ferretti, A.; Prati, C.; Rocca, F. Nonlinear subsidence rate estimation using permanent scatterers in differential SAR interferometry. *IEEE Trans. Geosci. Remote Sens.* **2000**, *38*, 2202–2212. [[CrossRef](#)]
71. Fárová, K.; Jelének, J.; Kopačková-Strnadová, V.; Kycl, P. Comparing DInSAR and PSI techniques employed to Sentinel-1 data to monitor highway stability: A case study of a massive Dobkovičky landslide, Czech Republic. *Remote Sens.* **2019**, *11*, 2670. [[CrossRef](#)]
72. Perissin, D. Interferometric SAR multitemporal processing: Techniques and applications. In *Multitemporal Remote Sensing*; Springer: Berlin/Heidelberg, Germany, 2016; pp. 145–176.

73. Ahmad, A.; Sultan, M.; Falak, A. Urban subsidence monitoring by PSInSAR and its causes in Lahore, Pakistan. In Proceedings of the 2021 SAR in Big Data Era (BIGSAR DATA), Nanjing, China, 22–24 September 2021; pp. 1–4.
74. Malik, A. Geotechnical Statistical Evaluation of Lahore Site Data and Deep Excavation Design. Master's Thesis, Portland State University, Portland, OR, USA, 2015.
75. Ahmad, N.; Ahmad, M.; Rafiq, M.; Iqbal, N.; Ali, M.; Sajjad, M.I. Hydrological modeling of the Lahore-Aquifer, using isotopic, chemical and numerical techniques. *Back Issues J. Sci. Vis.* **2002**, *7*, 16.
76. Holzer, T.L.; Johnson, A.I. Land subsidence caused by ground water withdrawal in urban areas. *GeoJournal* **1985**, *11*, 245–255. [[CrossRef](#)]
77. Hassan, G.Z.; Hassan, F.R.; Akhtar, S. Environment threats to groundwater in Lahore area. In Proceedings of the Pakistan Engineering Congress World Environment Day, Lahore, Pakistan, 5 June 2014; pp. 68–98.
78. Wang, Y.-Q.; Wang, Z.-F.; Cheng, W.-C. A review on land subsidence caused by groundwater withdrawal in Xi'an, China. *Bull. Eng. Geol. Environ.* **2019**, *78*, 2851–2863. [[CrossRef](#)]
79. Figueroa-Miranda, S.; Tuxpan-Vargas, J.; Ramos-Leal, J.A.; Hernández-Madrugal, V.M.; Villaseñor-Reyes, C.I. Land subsidence by groundwater over-exploitation from aquifers in tectonic valleys of Central Mexico: A review. *Eng. Geol.* **2018**, *246*, 91–106. [[CrossRef](#)]
80. Ullah, Z.; Talib, M.A.; Rashid, A.; Ghani, J.; Shahab, A.; Irfan, M.; Rauf, A.; Bawazeer, S.; Almarhoon, Z.M.; Mabkhot, Y.N.J.W. Hydrogeochemical investigation of elevated arsenic based on entropy modeling, in the aquifers of District Sanghar, Sindh, Pakistan. *Water* **2021**, *13*, 3477. [[CrossRef](#)]
81. Meribole, J. The Water Crisis in Pakistan. In *Borgen Magazine; The Borgen Project*: Seattle, WA, USA, 2020.
82. Jo, M.-J.; Won, J.-S.; Kim, S.-W. A time-series observation of ground subsidence at Ulsan area using SAR interferometry. In Proceedings of the 2011 3rd International Asia-Pacific Conference on Synthetic Aperture Radar (AP SAR), Seoul, Korea, 26–30 September 2011; pp. 1–3.
83. Ge, D.; Wang, Y.; Zhang, L.; Li, M.; Guo, X. Integrating medium and high resolution psinsar data to monitor terrain motion along large scale manmade linear features—A case study in shanghai. In Proceedings of the 2013 IEEE International Geoscience and Remote Sensing Symposium-IGARSS, Melbourne, Australia, 21–26 July 2013; pp. 4034–4037.
84. Osmanoğlu, B.; Dixon, T.H.; Wdowinski, S.; Cabral-Cano, E.; Jiang, Y. Mexico City subsidence observed with persistent scatterer InSAR. *Int. J. Appl. Earth Obs. Geoinf.* **2011**, *13*, 1–12. [[CrossRef](#)]
85. Liu, X.; Wang, Z.; Huang, R. Prediction on carbon emissions trend in Beijing Tianjing and Hebei Province. In Proceedings of the 2011 19th International Conference on Geoinformatics, Shanghai, China, 24–26 June 2011; pp. 1–4.
86. Galloway, D.L.; Burbey, T.J. Regional land subsidence accompanying groundwater extraction. *Hydrogeol. J.* **2011**, *19*, 1459–1486. [[CrossRef](#)]
87. Iqbal, J.; Su, C.; Rashid, A.; Yang, N.; Baloch, M.Y.J.; Talpur, S.A.; Ullah, Z.; Rahman, G.; Rahman, N.U.; Sajjad, M.M. Hydrogeochemical assessment of groundwater and suitability analysis for domestic and agricultural utility in Southern Punjab, Pakistan. *Water* **2021**, *13*, 3589. [[CrossRef](#)]
88. Kaplan, G.; Avdan, Z.Y. Space-borne air pollution observation from sentinel-5p tropomi: Relationship between pollutants, geographical and demographic data. *Int. J. Eng. Geosci.* **2020**, *5*, 130–137. [[CrossRef](#)]
89. Jat Baloch, M.Y.; Zhang, W.; Chai, J.; Li, S.; Alqurashi, M.; Rehman, G.; Tariq, A.; Talpur, S.A.; Iqbal, J.; Munir, M. Shallow Groundwater Quality Assessment and Its Suitability Analysis for Drinking and Irrigation Purposes. *Water* **2021**, *13*, 3361. [[CrossRef](#)]
90. Rana, I.A.; Bhatti, S.S. Lahore, Pakistan—Urbanization challenges and opportunities. *Cities* **2018**, *72*, 348–355. [[CrossRef](#)]
91. Tahir, A.A.; Muhammad, A.; Mahmood, Q.; Ahmad, S.S.; Ullah, Z. Impact of rapid urbanization on microclimate of urban areas of Pakistan. *Air Qual. Atmos. Health* **2015**, *8*, 299–306. [[CrossRef](#)]
92. Nof, R.N.; Baer, G.; Ziv, A.; Raz, E.; Atzori, S.; Salvi, S. Sinkhole precursors along the Dead Sea, Israel, revealed by SAR interferometry. *Geology* **2013**, *41*, 1019–1022. [[CrossRef](#)]